We are IntechOpen, the world's leading publisher of Open Access books Built by scientists, for scientists

4,800
Open access books available

122,000
International authors and editors

135M
Downloads

Our authors are among the

154
Countries delivered to

TOP 1%
most cited scientists

12.2%
Contributors from top 500 universities

CLARIVATE ANALYTICS BOOK CITATION INDEX INDEXED

WEB OF SCIENCE™

Selection of our books indexed in the Book Citation Index in Web of Science™ Core Collection (BKCI)

Interested in publishing with us?
Contact book.department@intechopen.com

Numbers displayed above are based on latest data collected.
For more information visit www.intechopen.com

10

Robust LMI-Based PID Controller Architecture for a Micro Cantilever Beam

Marialena Vagia and Anthony Tzes
University of Patras, Electrical and Computer Engineering Department
Greece

1. Introduction

Electrostatic Micro-Electro-Mechanical Systems (MEMS), are mechanical structures, consisting of mechanical moving parts actuated by externally induced electrical forces (Towfighian et al., 2011). The use of electrostatic actuation, is interesting, because of the high energy densities and large forces developed in such microscale devices (Chu et al., 2009; Vagia & Tzes, 2010b). For that reason, electrostatic micro actuators have been used in the fabrication of many devices in recent years, such as capacitive pressure sensors, comb drivers, micropumps, inkjet printer heads, RF switches and vacuum resonators.

Amongst different types of electrostatic micro actuators (Towfighian et al., 2010), electrostatic micro cantilever beams ($E\mu Cbs$) are considered as the most popular resonators. They can be extremely useful for a wide variety of tuning applications such as atomic force microscope (AFM), sensing sequence-specific DNA, detection of single electron spin, mass and chemical sensors, hard disk drives etc.

Accurate modeling of $E\mu Cb$s can be a challenging task, since such micro-systems suffer from nonlinearities that are due to the structural characteristics, the electrostatic force and the mechanical-electrical effects that are present. In addition, there exist more effects that play a dominant role especially in systems of narrow micro cantilever beams undergoing large deflections (Rottenberg et al., 2007). In such structures, the effects of the fringing fields on the electrostatic force are not negligible because of the non zero thickness and finite width of the beam (Gorthi et al., 2004; Younis et al., 2003). Thus, the incorporation of the fringing field capacitance, while modeling $E\mu Cb$s is mandatory. In that case the inclusion of the effects of the fringing field capacitance gives a more complicated but on the other hand a more accurate model of the cantilever beams.

Another important phenomenon appears with the interaction of the nonlinear electrostatic force with the linear elastic restoring one, and is called the “pull-in" phenomenon preventing the electrodes from being stably positioned over a large distance. The “pull-in" phenomenon restricts the allowable displacement of the moving electrodes in $E\mu Cb$'s systems operating in open-loop mode. For that reason, extending the travel range of $E\mu Cb$s is essential, in many practical applications including optical switches, tunable laser diodes, polychromator gratings, optical modulators and millipede data storage systems (Cheng et al., 2004; Towfighian et al., 2010). In order to achieve this extension in attracting mode beyond the conventional one-third of the capacitor beam’s gap, researchers have used various methods including charge and current control, and leveraged bending. However, despite the different

control approaches proposed until now (Nikpanah et al., 2008; Vagia & Tzes, 2010b), the control scheme to be applied on a micro-structure needs to be simple enough in order to be realizable in CMOS technology so that it can be fabricated on the same chip, next to switch.

In the present study, rather than relying on the design of non–linear control schemes, simplified linear optimal robust controllers (Sung et al., 2000; Vagia et al., 2008) are proposed. The design relies on the linearization of the $E\mu CB$'s nonlinear model at various multiple operating points, prior to the design of the control technique. For the resulting multiple linearized models of the $E\mu Cb$ a combination of optimal robust advanced control techniques in conjunction with a feedforward compensator are essential, in order to achieve high fidelity control of this demanding structure of the $E\mu Cb$ system. The proposed control architecture, relies on a robust time-varying PID controller. The controller's parameters are tuned within an LMI framework. A set of linearized neighboring sub–systems of the nonlinear model are examined in order to calculate the controller's gains. These gains guarantee the local stability of the overall scheme despite any switching between the linearized systems according to the current operating point. In order to enhance the performance of the closed–loop system, a set of PID controllers can be provided. The switching amongst members of the set of the PID controllers depends on the operating point. Each member of this set stabilizes the current linearized system and its neighboring ones. Through this overlapping stabilization of the linearized systems, the $E\mu Cb$'s stability can be enhanced even if the dwell time is not long enough.

The rest of this article is organized as follows, the modelling procedure for a $E\mu Cb$ is presented in Section 2. In Section 3, the proposed controller design procedure is described while in Section 4 simulation studies are carried, in order to prove the effectiveness of the proposed control technique. Finally in Section 5 the Conclusions are drawn.

2. Modeling of the electrostatic micro cantilever beam with fringing effects

The electrostatically actuated $E\mu CB$ is an elastic beam suspended above a ground plate, made of a conductive material. The cantilever beam moves under the actuation of an externally induced electrostatic force. The conceptual geometry of an electrostatic actuator composed of a cantilever beam separated by a dielectric spacer of the fixed ground plane is shown in Figure 1.

In the above Figure, ℓ, w, h are the length, the width and the thickness of the beam, η is the vertical displacement of the free end end from the relaxed position, and $\eta^{\max}$ is the initial thickness of the airgap between the moving electrode and the ground and F_{el} is the electrically-induced force between the two electrodes (Sun et al., 2007; Vagia & Tzes, 2010a).

The governing equation of motion of the $E\mu CB$ presented in Figure 1, is obtained, if considering that the mechanical force of the beam is modeled in a similar manner to that of a parallel plate capacitor with a spring and damping element (Batra et al., 2006; Pamidighantam et al., 2002).

The dynamical equation of motion due to the mechanical, electrostatic and damping force is equal to:

$$m\ddot{\eta} + b\dot{\eta} + k\eta = F_{el} \tag{1}$$

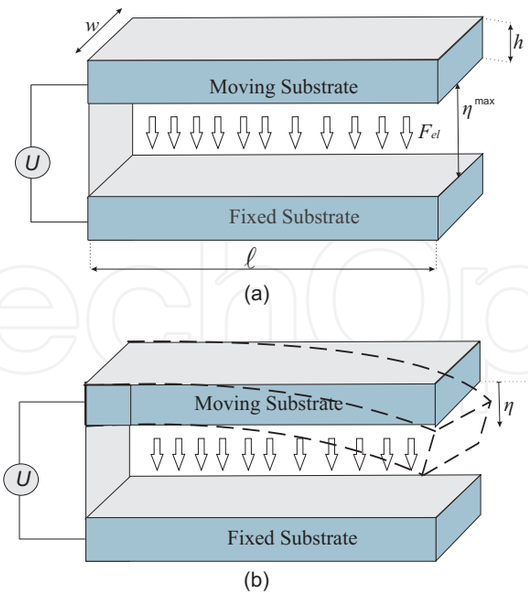

Fig. 1. Electrostatic Micro Cantilever Beam architecture

where m is the beam's mass, k is the spring's stiffness, b is the damping caused by the motion of the beam in the air.

2.1 Electrical force model

In a system of an $E\mu Cb$ composed of a cantilever beam separated by a dielectric spacer from the ground, the developed electrostatic force pulls the beam towards to the fixed ground plane as presented in Figure 1(b). The electrostatic attraction force F_{el} can be found by differentiating the stored energy between the two electrodes with respect to the position of the movable beam and can be expressed as (Batra et al., 2006; Chowdhury et al., 2005):

$$F_{el} = -\frac{d}{d\eta}\left(\frac{1}{2}CU^2\right) \tag{2}$$

where C is the $E\mu Cb$'s capacitance and U is the applied voltage between the beam's two surfaces.

The cantilever beam shown in Figure 1 can be viewed as a semi-infinitely VLSI on-chip interconnect separated from a ground plane (substrate) by a dielectric medium (air). If the bandwidth-airgap ratio is smaller than 1.5, the fringing field component becomes the dominant one.

The capacitance C in Equation (2), can be written as (Rottenberg et al., 2007):

$$C = e_0 e_r \ell\left(\frac{w}{\eta^{\max}}\right) + 0.77 e_0 \ell + 1.06 e_0 e_r \ell\left(\frac{w}{(\eta^{\max}-\eta)}\right)^{0.25} + 1.06 e_0 e_r \ell\left(\frac{h}{(\eta^{\max}-\eta)}\right)^{0.5} + 1.06 e_0 e_r w\left(\frac{\ell}{\eta^{\max}-\eta}\right)^{0.25} \tag{3}$$

where e_0 is the permittivity of the free space and e_r is the dielectric constant of the air.

The first term on the right-hand side of Equation (3), describes the parallel-plate capacitance, the third term expresses the fringing field capacitance due to the interconnect width w, the fourth term captures the fringing field capacitance due to the interconnect thickness h and the fifth expresses the fringing field capacitance due to the interconnect length ℓ as shown in Figure 2.

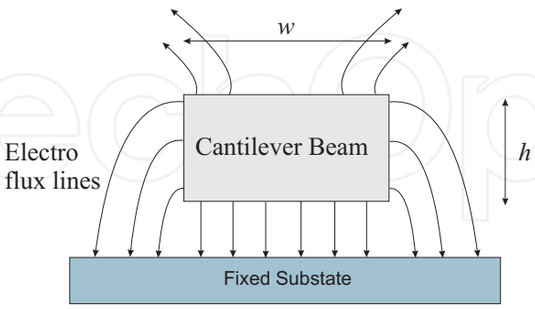

Fig. 2. Electric flux lines between the cantilever beam and the ground plane

After performing the differentiation of Equation (2) the electrical force is equal to:

$$F_{el} = \frac{e_0 w \ell U^2}{2(\eta^{\max} - \eta)^2} + \frac{0.1325 e_0 w^{0.25} \ell U^2}{(\eta^{\max} - \eta)^{1.25}} + \frac{0.265 e_0 h^{0.5} \ell U^2}{(\eta^{\max} - \eta)^{1.5}} + \frac{0.1325 e_0 w \ell^{0.25} U^2}{(\eta^{\max} - \eta)^{1.25}}. \tag{4}$$

The nonlinear equation of motion incorporating the expressions of the electrical and mechanical forces applied on the beam, is presented in Equation (5) as follows:

$$m\ddot{\eta} + b\dot{\eta} + k\eta = \frac{e_0 w \ell U^2}{2(\eta^{\max} - \eta)^2} + \frac{0.1325 e_0 w^{0.25} \ell U^2}{(\eta^{\max} - \eta)^{1.25}} + \frac{0.265 e_0 h^{0.5} \ell U^2}{(\eta^{\max} - \eta)^{1.5}} + \frac{0.1325 e_0 w \ell^{0.25} U^2}{(\eta^{\max} - \eta)^{1.25}}. \tag{5}$$

2.2 Linearized equations of motion

Equation (5) is a nonlinear equation due to the presence of the parameters η and U. All possible "equilibria"-points η_i^o, $i = 1, \ldots, M$ depend on the applied nominal voltage U_o. Equation (5) for $\ddot{\eta}_i^o = \dot{\eta}_i^o = 0$ and η_i^o yields:

$$k\eta_i^o = \underbrace{\frac{e_0 \ell w}{2(\eta^{\max} - \eta_i^o)^2}}_{k_{11}} U_o^2 + \underbrace{\frac{0.1325 e_0 \ell w^{0.25}}{(\eta^{\max} - \eta_i^o)^{1.25}}}_{k_{22}} U_o^2 + \underbrace{\frac{0.265 e_0 \ell h^{0.5}}{(\eta^{\max} - \eta_i^o)^{1.5}}}_{k_{33}} U_o^2 + \underbrace{\frac{0.1325 e_0 \ell^{0.25} w}{(\eta^{\max} - \eta_i^o)^{1.25}}}_{k_{44}} U_o^2 \Leftrightarrow$$

$$U_o = \pm \left[\frac{k\eta_i^o}{k_{11} + k_{22} + k_{33} + k_{44}} \right]^{1/2} \tag{6}$$

This nominal Uo-voltage must be applied if the beam's upper electrode is to be maintained at a distance $\eta_i^o \leq \frac{\eta^{\max}}{3}$ from its un-stretched position and equals to the feedforward compensator. This fact must be taken into account, as in the presented system, the "pull-in" phenomenon exists resulting to a single bifurcation point at $\eta^b = \frac{\eta^{\max}}{3}$. The resulting linearized systems

that exist below this point are stable, while the linearized sub-systems above this limit are unstable. In the sequel Uo voltage, that keeps the system at η^b and will be referred to as the "bifurcation parameter".

The linearized equations of motion around the equilibria points $\left(U_o,\ \eta_i^o, \text{and } \ddot{\eta}_i^o = \dot{\eta}_i^o = 0\right)$ can be found using standard perturbation theory for the variables U and η_i where $U = U_o + \delta u$ $\eta_i = \eta_i^o + \delta\eta_i$. The linearized equation can be described as:

$$m\delta\ddot{\eta}_i + b\dot{\eta}_i + k\delta\eta_i + k\eta_i^o = \frac{e_0\ell w U_o^2}{2(\eta^{\max} - \eta_i^o)^2} + \frac{e_0 w\ell U_o^2}{(\eta^{\max} - \eta_i^o)^3}\delta\eta_i + \frac{e_0 w\ell U_o}{(\eta^{\max} - \eta_i^o)^2}\delta u + \frac{0.1325 e_0\ell w^{0.25} U_o^2}{(\eta^{\max} - \eta_i^o)^{1.25}} +$$

$$\frac{0.165 e_0 w^{0.25}\ell U_o^2}{(\eta^{\max} - \eta_i^o)^{2.25}}\delta\eta_i + \frac{0.265 e_0 w^{0.25}\ell U_o}{(\eta^{\max} - \eta_i^o)^{1.25}}\delta u + \frac{0.265 e_0\ell h^{0.5} U_o^2}{(\eta^{\max} - \eta_i^o)^{1.5}} + \frac{0.397 e_0 h^{0.5}\ell U_o^2}{(\eta^{\max} - \eta_i^o)^{2.5}}\delta\eta_i + \frac{0.53 e_0 h^{0.5}\ell U_o}{(\eta^{\max} - \eta_i^o)^{1.5}}\delta u +$$

$$\frac{0.1325 e_0\ell^{0.25} w U_o^2}{(\eta^{\max} - \eta_i^o)^{1.25}} + \frac{0.1625 e_0 w\ell^{0.25} U_o^2}{(\eta^{\max} - \eta_i^o)^{2.25}}\delta\eta_i + \frac{0.265 e_0 w\ell^{0.25} U_o}{(\eta^{\max} - \eta_i^o)^{1.25}}\delta u,\ \ i = 1, \ldots, M.$$

Substitution of:

$$k_i^a = k - \frac{e_0 w\ell U_o^2}{(\eta^{\max} - \eta_i^o)^3} - \frac{0.165 e_0 w^{0.25}\ell U_o^2}{(\eta^{\max} - \eta_i^o)^{2.25}} - \frac{0.397 e_0 h^{0.5}\ell U_o^2}{(\eta^{\max} - \eta_i^o)^{2.5}} - \frac{0.1625 e_0 w\ell^{0.25} U_o^2}{(\eta^{\max} - \eta_i^o)^{2.25}}$$

$$\beta_i = \frac{e_0 w\ell U_o}{(\eta^{\max} - \eta_i^o)^2} + \frac{0.265 e_0 w^{0.25}\ell U_o}{(\eta^{\max} - \eta_i^o)^{1.25}} + \frac{0.53 e_0 h^{0.5}\ell U_o}{(\eta^{\max} - \eta_i^o)^{1.5}} + \frac{0.265 e_0 w\ell^{0.25} U_o}{(\eta^{\max} - \eta_i^o)^{1.25}}, i = 1, \ldots, M.$$

yields to the final set of linearized equations describing the nonlinear system, for all different operating points:

$$m\delta\ddot{\eta}_i + b\delta\dot{\eta}_i + k_i^a\delta\eta_i = \beta_i\delta u, M = 1, \ldots, M. \tag{7}$$

The equations of motion describing the linearized subsystems, in state space form are equal to:

$$\begin{bmatrix} \delta\dot{\eta}_i \\ \delta\ddot{\eta}_i \end{bmatrix} = \begin{bmatrix} 0 & 1 \\ \frac{-k_i^a}{m} & \frac{-b}{m} \end{bmatrix} \begin{bmatrix} \delta\eta_i \\ \delta\dot{\eta}_i \end{bmatrix} + \begin{bmatrix} 0 \\ \frac{\beta_i}{m} \end{bmatrix} \delta u = \tilde{A}_i \begin{bmatrix} \delta\eta_i \\ \delta\dot{\eta}_i \end{bmatrix} + B_i\delta u,\ \ i = 1, \ldots, M$$

$$\delta\eta_i = [1\ \ 0] \begin{bmatrix} \delta\eta_i \\ \delta\dot{\eta}_i \end{bmatrix} = C \begin{bmatrix} \delta\eta_i \\ \delta\dot{\eta}_i \end{bmatrix}, i = 1, \ldots, M. \tag{8}$$

3. Switching robust control design

The design aspects of the used robust switching (Ge et al., 2002; Lam et al., 2002) LMI–based PID–controller comprised of $N + 1$ "switched" PID sub-controllers, coupled to a feedforward controller (FC), as shown in Figure 3, will be presented in this Section.

The feedforward term provides the voltage U_0 from Equation (6) while the robust switching PID controller for the set of the M–linearized systems in Equation (8) is tuned via the utilization of LMIs (Boyd et al., 1994) and a design procedure based on the theory of Linear Quadratic Regulators (LQR).

This robust switching PID–controller is specially designed to address the case where multiple–system models have been utilized (Chen, 1989; Cheng & Yu, 2000; Hongfei & Jun, 2001; Narendra et. al., 1995; Pirie & Dullerud, 2002; Vagia et al., 2008) in order to describe the uncertainties that are inherent from the linearization process of the nonlinear system model.

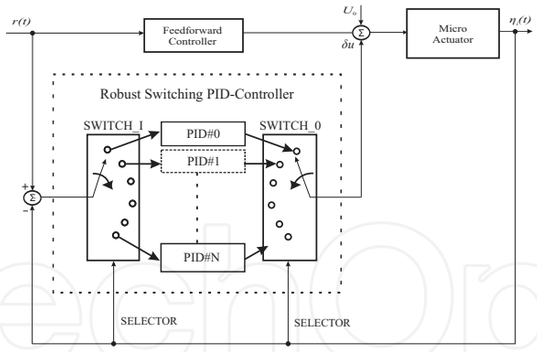

Fig. 3. Feedforward and Switching PID Control Architecture

The nature of the PID–structure in the controller design can be achieved if the linearized system's state vector $\delta\bar{\eta}_i = [\delta\eta_i, \delta\dot{\eta}_i]^T$ is augmented with the integral of the error signal $\int e_i dt = \int (r(t) - \eta_i(t))\, dt$. In this case, the augmented system's description is

$$\begin{bmatrix} \delta\dot{\bar{\eta}}_i \\ -e_i \end{bmatrix} = \hat{A}_i \begin{bmatrix} \delta\bar{\eta}_i \\ -\int e_i dt \end{bmatrix} + \begin{bmatrix} B_i \\ 0 \end{bmatrix} \delta u + \begin{bmatrix} -1 \\ 0 \end{bmatrix} r, \tag{9}$$

where $\hat{A}_i = \begin{bmatrix} \tilde{A}_i & 0 \\ 1 & 0 \end{bmatrix}$.

The LQR–problem for each system $(i = 0, \ldots, M)$ described in Equation (9) can be cast in the computation of δu in order to minimize the following cost:

$$J(\delta u) = \int_0^\infty (\delta\tilde{\eta}_i{}^T\, Q\, \delta\tilde{\eta}_i + \delta u^T\, R\, \delta u) dt \tag{10}$$

where $\delta\tilde{\eta}_i = \left[\delta\bar{\eta}_i, -\int e_i dt\right]^T$ is the state vector of the augmented system, and Q, R are semidefinite and definite matrices respectively. If a single PID-controller was desired ($N = 0$), then the solution to the LQR problem relies on computing a common Lyapunov matrix that satisfies the Algebraic Ricatti Equations (AREs):

$$\hat{A}_i{}^T P + P\hat{A}_i - PB_i R^{-1} B_i{}^T P + Q = 0, i = 0, \ldots, M. \tag{11}$$

Rather than using the $\hat{A}_i$–matrices in the LQR–problem, the introduction of the auxiliary matrices $A_i = \hat{A}_i + \Lambda\mathbf{I}$, where $\Lambda > 0$ and $\mathbf{I}$ the identity matrix generates an optimal control $\delta u = -S\delta\tilde{\eta}$ such that the closed–loop's poles have real part less than $-\Lambda$, or $\Re(\mathrm{eig}(\hat{A}_i - B_i S)) < -\Lambda\ \forall i \in \{0, \ldots, M\}$.

The switching nature of the PID–controller is based on the following principle. Under the assumption of $M + 1$ linearized systems and $N + 1$ available PID controllers ($N \leq M$), the objective of $\jmath$th PID–controller is to stabilize the $\jmath$–th system $\jmath \in \{0, \ldots, N\}$ and its 2Δ-neighboring ones $\jmath - \Delta, \ldots, \jmath - 1, \jmath, \jmath + 1, \ldots, \jmath + \Delta$, where Δ is an ad-hoc designed parameter related to the range of the affected neighboring subsystems.

If the stability-issue is the highest consideration, thus allowing for increased conservatism, only one ($N + 1 = 1$) controller is designed for all $M + 1$ subsystems, or $\jmath - \frac{M}{2}, \ldots, \jmath, \ldots, \jmath + \frac{M}{2}$ (under the assumption that $\Delta = \frac{M}{2}$). This fixed time–invariant controller ($\delta u = -S\delta\tilde{\eta}$)

stabilizes any linearized system (A, B) within the convex hull defined by the $(A_i, B_i), i = 0, \ldots, M$ vertices, or $(A, B) \in \text{Co}\{(A_0, B_0), \ldots, (A_M, B_M)\}$.

There is no guarantee, that this fixed linear time–invariant controller when applied to the nonlinear system will stabilize it, nor that it can stabilize the set of all linearized systems when switchings of the control occur. The promise is that when there is a slow switching process, then this single PID controller will stabilize any switched linear system $(A(t), B(t)) \in \text{Co}\{(A_i, B_i), i = 0, \ldots, M\}$.

Furthermore if M increases then the approximation of the nonlinear system by a large number of linearized systems is more accurate. This allows the interpretation of the solution to the system's nonlinear dynamics

$$\delta\dot{\tilde{\eta}} = f(\delta\tilde{\eta}) + g(\eta, \delta u) \tag{12}$$

as a close match to the solution of the system's time-varying linearized dynamics

$$\delta\dot{\tilde{\eta}} = A(t)\delta\tilde{\eta} + B(t)\delta u. \tag{13}$$

The increased conservatism stems from the need to stabilize a large number of systems with a single controller, thus limiting the performance of the closed loop system.

In order to enhance the system's performance, multiple controllers can be used; each controller needs not only to stabilize the current linearized system but also its neighboring ones thus providing increased robustness against switchings at the expense of sacrificing the system's performance.

In a generic framework, the $\jmath$th robust switching–PID controller's objective is to optimize the cost in (10) while the $\jmath$th–linearized system is within

$$\text{Co}\{(A_i, B_i), i \in \{\jmath - \Delta, \ldots, \jmath + \Delta\}\}. \tag{14}$$

Henceforth , the needed modification to (11) is the adjustment of the spam of the systems from $\{0, \ldots, M\}$ to $\{\jmath - \Delta, \ldots, \jmath + \Delta\}$. It should be noted that the optimal cost at Equation (10) is equal to $\delta\tilde{\eta}^T(0)\hat{P}^{-1}\delta\tilde{\eta}(0)$ for a P-matrix satisfying (11). An efficient alternative solution for the optimal control $\delta u = -S\delta\tilde{\eta}$ can be computed by transforming the aforementioned optimization problem, subject to the concurrent satisfaction of the AREs in Equation (11), into an equivalent LMI–based algorithm, where a set of auxiliary matrices $\hat{P}$, Y and an additional variable γ $(\gamma > 0)$ have been introduced.

The γ–variable is used as an upper bound of the cost, or

$$\delta\tilde{\eta}^T(0)\hat{P}^{-1}\delta\tilde{\eta}(0) \leq \gamma. \tag{15}$$

Therefore the optimal control problem amounts to the minimization of γ subject to the satisfaction of the AREs in (11). The optimal control $\delta u = -S\delta\tilde{\eta}$ is encapsulated in the following formulation which is amenable for solution via classical LMI–based algorithms; relying on Schur's complement (Boyd et al., 1994), and the introduction of a set of auxiliary matrices $\hat{P}$, Y and an additional variable γ $(\gamma > 0)$ the controller computation problem is transformed to:

$$\min \gamma$$

$$\text{subject to} \begin{cases} \begin{bmatrix} \gamma & \delta\tilde{\eta}^T(0) \\ \delta\tilde{\eta}(0) & \hat{P} \end{bmatrix} \leq 0 \\ \begin{bmatrix} A_i\hat{P} + \hat{P}A_i^T + B_iY + Y^TB_i^T & \hat{P} & Y^T \\ \hat{P} & -Q^{-1} & 0 \\ Y & 0 & -R^{-1} \end{bmatrix} \leq 0 \ , \\ \text{for } i = \jmath - \Delta, \ldots, \jmath + \Delta \\ \hat{P} > 0 \ . \end{cases}$$

The feedback control can be computed based on the recorded values of $\hat{P}^*$ and Y^* for the last feasible solution:

$$\begin{aligned} \delta u = Y^*(\hat{P}^*)^{-1}\delta\tilde{\eta} = -S\delta\tilde{\eta} &= -\left[\, s_p \middle| s_d \middle| s_i \,\right] \begin{bmatrix} \delta\eta_i \\ \delta\dot{\eta}_i \\ -\int edt \end{bmatrix} \\ &= \left[s_p e + s_d\dot{e} + s_i \int edt \right] + \left[s_p\left(\eta_i^o - r\right) - s_d\dot{r} \right] . \end{aligned} \tag{16}$$

The first portion of the controller form in (16) is equivalent to that of a PID–controller. It should be noted that the operating points are

$$\eta_i{}^o = \eta_0{}^{\min} + \frac{\eta_M{}^{\max} - \eta_0{}^{\min}}{M} \cdot i = \eta_0{}^{\min} + W \cdot i, \ \ i = 0, \ldots, M, \tag{17}$$

where W is the distance related to the separation of the operating points. The $\jmath$th locally stabilizing PID controller stabilizes the linearized systems that are valid over the interval

$$\begin{aligned} \left[\eta_\jmath{}^{\min}, \eta_\jmath{}^{\max}\right) = &\left[\eta_{j-\Delta}^o - \frac{W}{2}, \eta_{j+\Delta}^o + \frac{W}{2}\right) \bigcup \cdots \bigcup \\ &\left[\eta_j^o - \frac{W}{2}, \eta_j^o + \frac{W}{2}\right) \bigcup \cdots \bigcup \left[\eta_{j+\Delta}^o - \frac{W}{2}, \eta_{j+\Delta}^o + \frac{W}{2}\right) . \end{aligned} \tag{18}$$

Essentially the resulting PID structure is equivalent to that of an overlapping decomposition controller. The region of validity for each controller with respect to the available travel distance of the $E\mu Cb$ appears in Figure 4. Small number of W and Δ lead to smaller regions of validity with insignificant overlapping (i.e., when $\Delta = 0$ there is no overlapping and each controller is responsible for the region $\left[\eta_j^o - \frac{W}{2}, \eta_j^o + \frac{W}{2}\right)$)

For the travel-distances where there is overlapping the PID-controller maintains its gains, and when the beam moves out of the boundaries of that region the PID controller readjusts its gains. To exemplify this issue, consider the motion of the $E\mu Cb$ as shown in Figure 5.

The controller's switching mechanism starts with the set of gains of the $(\jmath - 1)$th controller for $\eta(t) \in \left[\eta_{\jmath-2}^{\max}, \eta_{\jmath-1}^{\max}\right)$. At time $t = t_1$, when $\eta(t) = \eta_{\jmath-1}^{\max}$ the controller switches to its new $(\jmath)$th controller and maintains this set of gains till time t_2. For $t \geq t_2$, or when $\eta(t) \geq \eta_\jmath^{\max}$ the $(\jmath + 1)$th controller is activated, until time instant t_3 at which $\eta(t) = \eta_{\jmath+1}^{\min}$. For $t_3 < t \leq t_4$, or $\eta_{\jmath+1}^{\min} < \eta(t) \leq \eta_\jmath^{\min}$ the $(\jmath)$th controller is activated. It should be noted that each controller

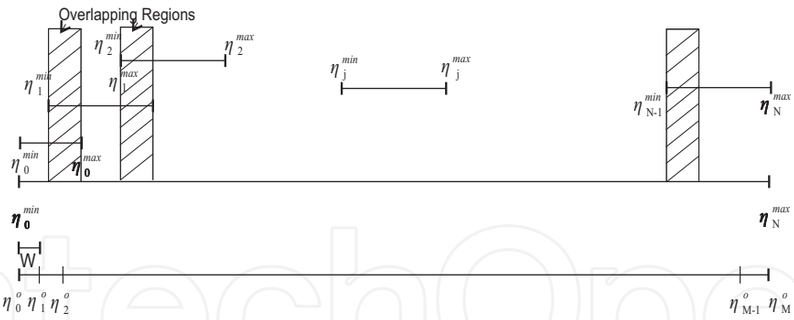

Fig. 4. Controllers' Regions of Validity

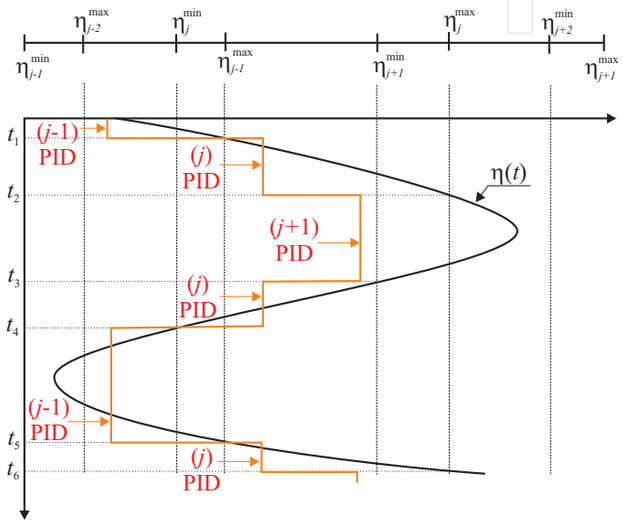

Fig. 5. PID- controller Gain Switching Example

is activated in a manner that resembles a "hysteresis"–effect. In the noted example, as $\eta(t)$ increases, the $\jmath$th controller operates when $\eta(t) \in \left[\eta_{\jmath-1}^{\max}, \eta_{\jmath}^{\max}\right)$, while as $\eta(t)$ decreases the same controller operates when $\eta(t) \in \left[\eta_{\jmath}^{\min}, \eta_{\jmath+1}^{\min}\right)$.

In the suggested framework the control design needs to select the number of:

1. the number $M+1$ of linearized systems (partitions)
2. the number $N+1$ of the switched controllers
3. the "width" Δ of the "overlapping system stabilizations" of each controller and
4. the cost Q, R parameters and the Λ factor used to "speed up" the system's response.

In general Q and R are given, and ideally M is desired to be as large as possible. As far as the three parameters N, Δ and Λ there is a trade–off in selecting their values. Large N-values lead to superfluous controller switchings which may destabilize the system; small N typically leads to a slow–responding system thus hindering its performance. Large values of Δ increase the system's stability margin while decreasing the system's bandwidth (due to the need to simultaneously stabilize a large number of systems). The parameter Λ directly affects the speed of the system's response. From a performance point of view, large Λ-values are desired; however this may lead to an infeasibility issue in the controller design.

It should be noted that a judicious selection of these parameters is desired, since there are contradicting outcomes behind their selection. As an example, large values of N leads to a faster performance at the expense of causing significant switchings caused by the transition of the controller's operating regime. Similarly, large values of Δ increase the systems's stability margin at the expense of decreasing its bandwidth which is also affected by the parameter Λ.

Practical considerations ask for an a priori selection of N and Δ while computing the largest Λ that generates a feasible controller.

4. Simulation studies

Simulation studies were carried on a $E\mu Cb$'s non–linear model. The parameters of the system unless otherwise stated are equal to those presented in the following Table.

parameter (Unit)	Description	Value
$w(m)$	Beam Width	7.5×10^{-6}
$h(m)$	Beam Height	1.2×10^{-6}
$\ell\ (m)$	Beam Length	100×10^{-6}
$\eta^{max}(m)$	Maximum Distance	4×10^{-6}
$\mu\ (kg\ m/sec^2)$	Viscosity Coefficient	18.5×10^{-6}
$\rho\ (kg/m^3)$	Density	1.155
$e_0\ (Coul^2/Nm^2)$	Dielectric constant of the air	8.85×10^{-12}
$P_a\ (N/m^2)$	Ambient Pressure	10^5
k (N/m)	Stiffness of the spring	0.249

The allowable displacements of the $E\mu Cb$ in the vertical axis: $\eta \in [0.1, 1.33]\ \mu$m=$[\eta_o^{\min}, \eta_M^{\max}]$. This is deemed necessary in order to guarantee the stability of the linearized open–loop system and retain it, below the well known-bifurcation points. These are the points where the behavior of the system changes from stable to unstable and vice versa and can be easily found by setting the derivative of $\frac{\partial U_o}{\partial \eta}$ of the expression in Equation (6) equal to zero. It should be noted that as presented at Figure 6, the bifurcation point is equal to the extrema of the graph presented, at $\eta^b = 1.33\mu m = \frac{\eta^{\max}}{3}$.

As far as the controller's design parameters are concerned, different test cases were examined in order to prove the effectiveness of the suggested control scheme. Different test cases, regarding the values of M, N, Δ, Λ are examined in order to prove the relevance between them and the system's performance.

Each set of the parameters of the controller switches at the instants, when: a) there is a movement of the upper plate from its initial to its final position, and b) at the crossings of the boundaries $\eta_i^{\min}, \eta_i^{\max}$ where each linearized model is valid.

Figure 7 presents the nonlinear system's responses for different Λ-values when a single robust PID controller is designed. The goal of the controller was to move the beam's upper plate from an initial position to a new desired one (set–point regulation). In this case, 5-linearized subsystems were used in each case for the controller's design, and thus $M = 5$ and $N = 0$. As expected, the system responds faster in the cases where the Λ-value is higher, since it is guaranteed that its closed–loop poles will be deeper in the LHP.

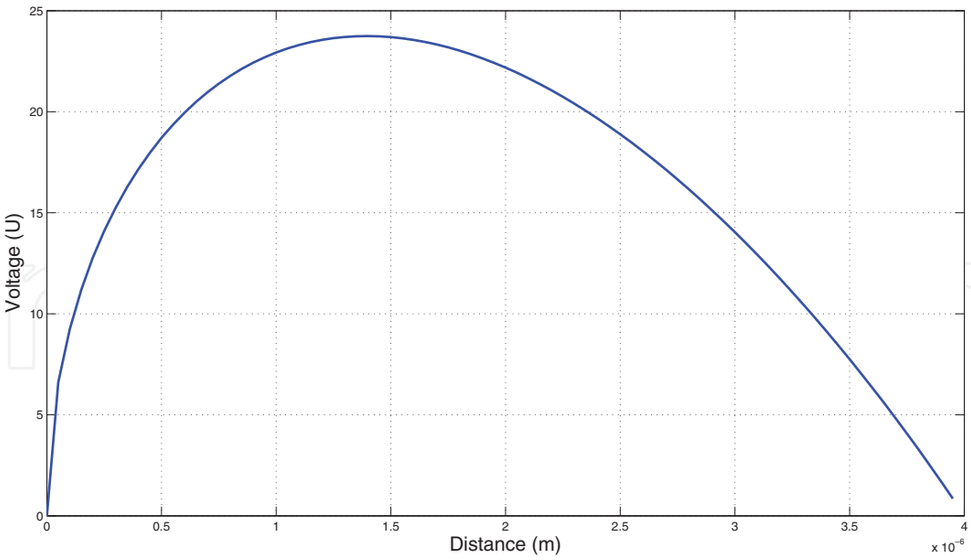

Fig. 6. Bifurcation points of the System

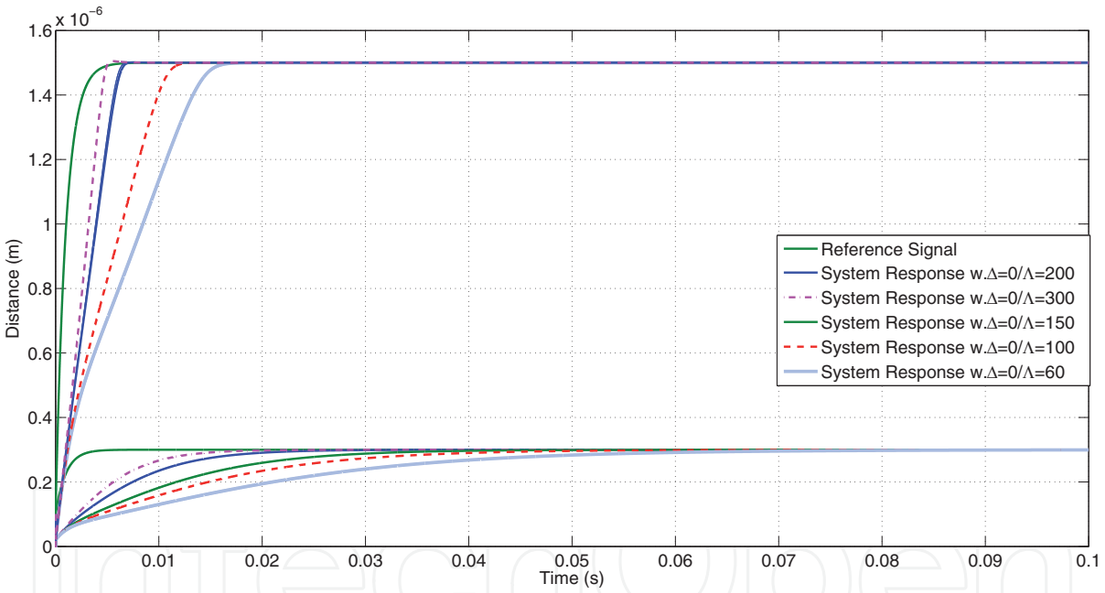

Fig. 7. Systems' Responses for different Λ-values

Another parameter to be examined is the number of the operating points (M value), and its effect on the system's performance. Figure 8 (9) presents the responses (control efforts) of the system when $M = 1, 5, 10$ and $N = 0$. Comparing the systems' responses in an apparent performance improvement is observed when using more operating points. However, due to the continuous switchings between the operating regimes, the control effort in the latter case ($M = 10$) is quite "noisy" and might cause significant aging on the beam's moving electrode.

In the sequel Figure 10 presents the responses of the system for different N-values ($N + 1 = 1, 4, 10$). The other parameters of the controller equal to: $\Delta = 0$ and $M = 5$ for all the three cases. The number of the switchings between the different designed PID-controllers

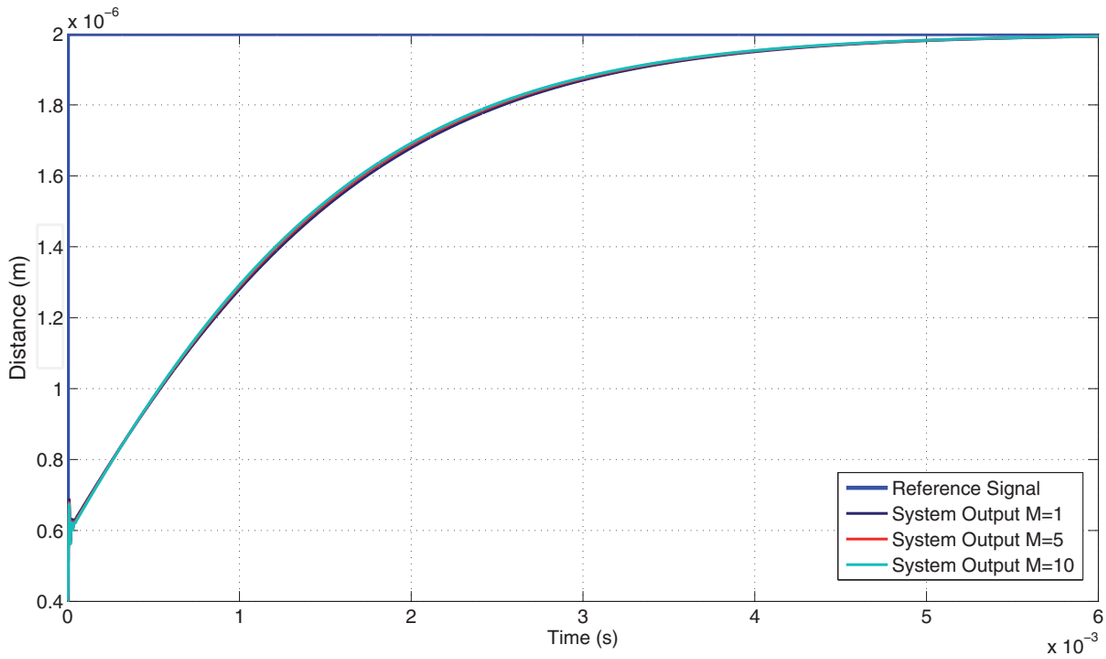

Fig. 8. Systems' Responses for different M values

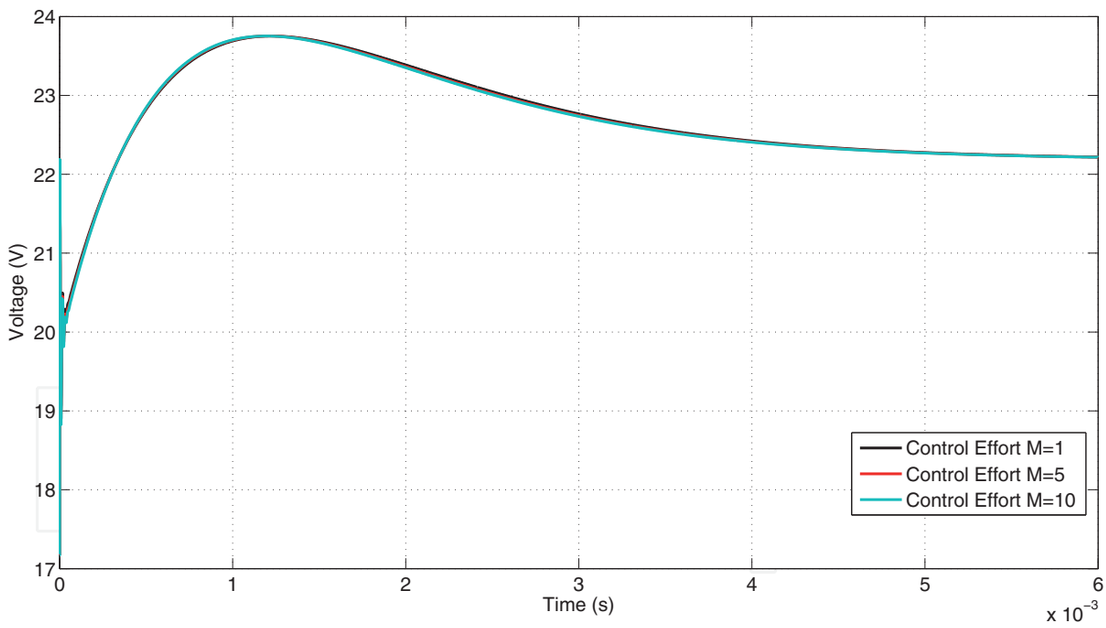

Fig. 9. Control Efforts for different M values

has a great impact on the system's output. The grater the number of N the faster the system becomes. On the other hand, an increase of N-values makes the system's response more oscillatory. Therefore the control law designed need to take into consideration, the trade off that exists between the velocity and the performance of the system when more controllers are used. Figure 11 presents the control efforts of the system that are in full harmony with the previous mentioned results.

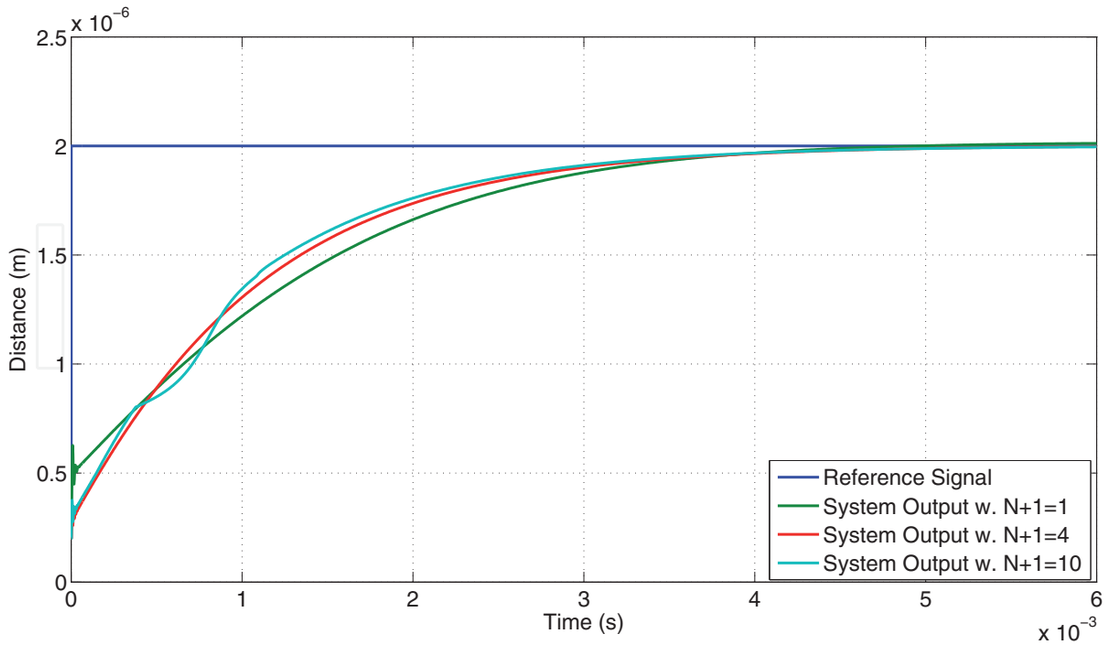

Fig. 10. Systems' Responses for different N-values

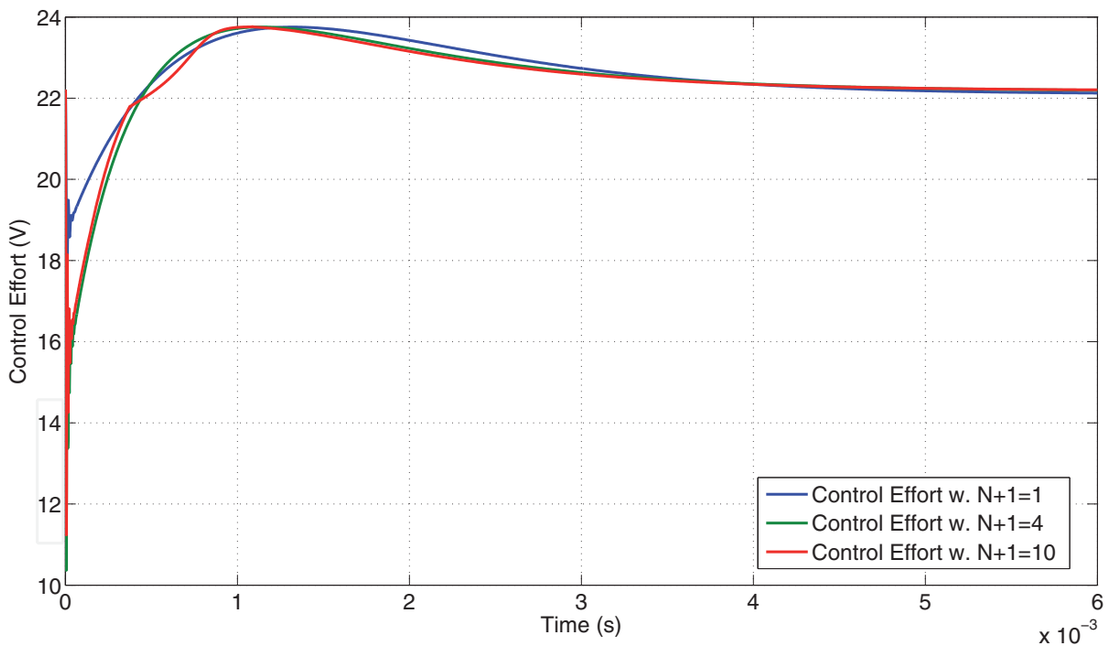

Fig. 11. Control Efforts for different N values

In Figure 12, the responses of the $E\mu Cb$'s non-linear model are presented for different values of Δ. Thirteen ($M+1$=14) operating points were selected at $\eta_i^o = \eta_0^{\min} + W \cdot i$, where $W = 0.1\mu m$ and $i \in \{0, \ldots, 13\}$. Three test-cases were examined as far as the number of the switched controllers: a) $N+1 = 13$, b) $N+1 = 9$ and c) $N+1 = 1$. For the first case there are no overlapping regions, thus ($\Delta = 0$). For the second case, there are three overlapping regions

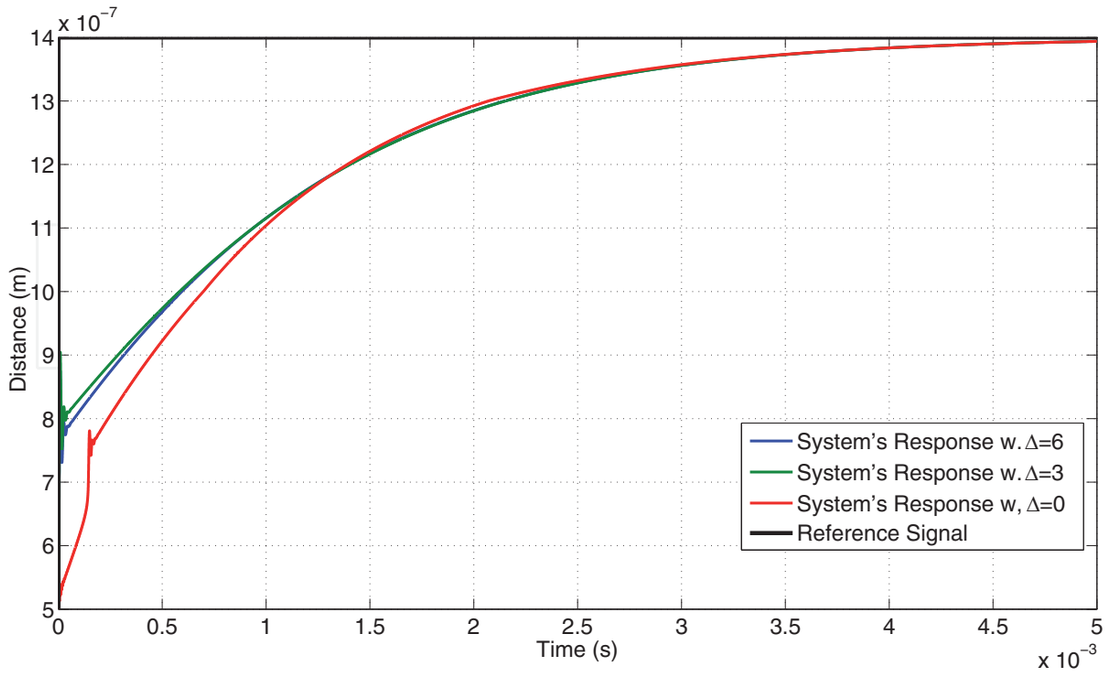

Fig. 12. Systems' Responses for different Δ values

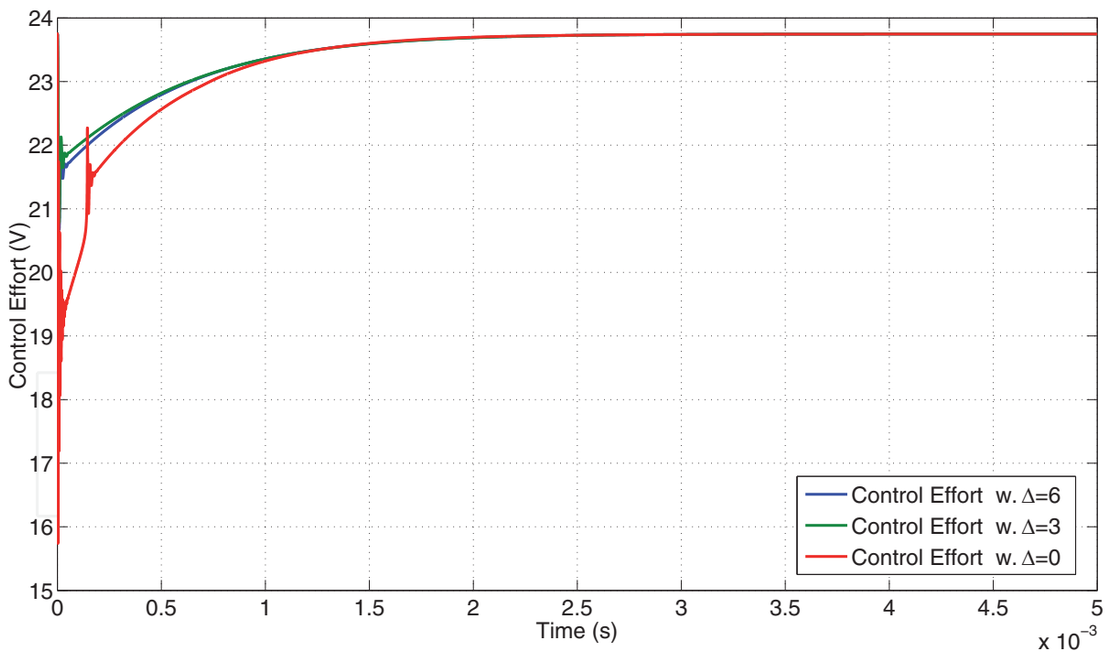

Fig. 13. Control Efforts for different Δ values

($\Delta = 3$) around each operating point. For the last case, where only one controller is used ($\Delta = 6$) this controller's region of validity is:

$$\left(\eta_6^0 - \Delta W - \frac{W}{2}, \eta_6^0 + \Delta W + \frac{W}{2}\right). \tag{19}$$

.

Figures 12 and 13 present the corresponding systems' responses and control efforts. In the cases where the Δ value is higher, the system's response becomes slower but the oscillations are diminished. This is also apparent from a direct comparison between the control effort shown in Figure 13.

5. Conclusion

In this article a robust switching control scheme is firstly designed, and then applied on the system of an $E\mu Cb$. The control architecture consisting of several robust switching PID controllers tuned with the utilization of the LMI technique, in conjunction with a feedforward term, is applied on the nonlinear beam's system. In an attempt to address the performance, the switching PID-controllers are designed in order to push the poles deep inside the LHP. The resulting scheme relies on a minimization procedure subject to the satisfaction of several LMI-constraints. Several test cases are provided in order to find any possible relevance between the different values used during the controller design procedure. Simulation studies prove the efficiency of the suggested scheme and highlight the provoked indirect effects caused by the frequency switchings of the time-varying control architecture.

6. References

Batra, R.C.; Porfiri, M. & Spinello, D. (2006). Capacitance estimate for electrostatically actuated narrow microbeams. *Micro & Nano Letters IET* Vol 1., No. 2., pp. 71-73.

Boyd, S.; Ghaoui, L.El; Feron, E. & Balakrishnan, V. (1994). Linear Matrix Inequalities in System and Control Theory. *SIAM*, Philadelphia, PA.

Chen C., (1989). A simple method for on-line identification and controller tuning. *AIChE*, Vol. 35., No. 12., pp. 2037–2039.

Cheng, Y. & Yu, C. (2000). Nonlinear process control using multiple models: relay feedback approach. *Industrial Eng.Chem*, Vol. 39., No. 2., pp. 420–431.

Cheng, J.; Zhe, J. & Wu, X. (2004). Analytical and finite element model pull-in study of rigid and deformable electrostatic microactuators. *Journal of Microelectronics and Microengineering*, Vol. 14., No. 1., pp. 57-68.

Chowdhury, S.; Ahmadi, M. & Mille, W. C. (2005). A closed-form model for the pull in voltage of electrostatically actuated cantilever beams. *Journal of Microelectronics and Microengineering*, Vol. 15., No. 4., pp. 756-763.

Chu, C, H.; Shih, W. P.; Chung, S. Y.; Tsai, H. C.; Shing, T. K. & Chang, P.Z. (2005). A low actuation voltage electrostatic actuator for RF MEMS switch applications. *Journal of Micromechanics and Microengineering*, Vol. 17., No.8., pp. 1649-1656.

Ge, M.; Chiu, M. & Wang, Q. (2002). Robust PID controller Design via LMI approach. *Journal of Process Control*, Vol. 12., No.1., pp. 3–13.

Gorthi, S.; Mohanty, A. & Chatterjee, A. (2004). Cantilever beam electrostatic MEMS actuators beyond pull-in. *Journal of Microelectronics and Microengineering*, Vol.14., No. 9., pp. 1800-1810.

Hongfei, S. & Jun, Z. (2001). Control Lyapunov functions for switched control systems. *Proceedings of the 2001 American Control Conference*, pp. 1890–1891, Arlington, Virginia, June 2001.

Lam, H. K.; Leung, F. H. F. & Tam, P. K. S. (2002). A switching controller for uncertain nonlinear systems. *IEEE Control System Magazine*, Vol. 22., pp. 7–14.

Narendra, K. S.; Balakrishnan, J. & Ciliz, K. (1995). Adaptation and Learning using multiple models, switching and tuning. *IEEE Control Systems Magazine*, Vol. 15., No. 3., pp. 37–51.

Nikpanah, M.; Wang, Y.; Lewis, F. & Liu, A. (2008). Real time controller design to solve the pull-in instability of MEMS actuator. *Proceedings of 10th Int. Conf. on Control, Automation, Robotics and Vision*, pp. 1724-1729, Hanoi, Vietnam.

Pamidighantam, S.; Puers, R.; Baert, K. & Tilmans, H. A. C. (2002). Pull in voltage analysis of electrostatically actuated beam structures with fixed-fixed and fixed-free end conditions. *Journal of Microelectronics and Microengineering*. Vol. 12., pp. 458-464.

Pirie, C. & Dullerud, G. (2002). Robust Controller synthesis for uncertain time-varying systems. *SIAM Journal on Control and Optimization*, Vol. 40. No. 4., pp. 1312-1331.

Rottenberg, X.; Brebels, S.; Ekkels, P.; Czarnecki, P.; Nolmans, P.; Mertens, R. P.; Nauwelaers, B.; Puers, R.; De Wolf, I.; De Raedt, W. & Tilmans, H. A. C. (2007). An electrostatic fringing-field actuator (EFFA): application towards a low-complexity thin-film RF-MEMS technology. *Journal of Micromechanics and Microengineering*. Vol. 17., No. 7., pp. 204-210.

Sun, D. M.; Dong, W.; Liu, C. X.; Chen, W. Y. & Kraft, M. (2007). Analysis of the dynamic behaviour of a torsional micro-mirror. *Journal of Microsystem Technology*. Vol. 13., No. 1., pp. 61-70.

Sung, L.; Yongsang, Q. K. & Dae-Gab, G. (2000). Continuous gain scheduling control for a micro-positioning system: Simple, robust and no overshoot responser. *Control Engineering Practice* Vol. 8., No. 2., pp. 133–138.

Towfighian, S.; Seleim, A.; Abdel-Rahman, E. M. & Heppler, G. R. (2010) Experimental validation for an extended stability electrostatic actuator. *Proceedings of ASME 2010 Int. Design Engineering Technical Conference.*, Montreal, QC, Canada .

Towfighian, S.; Seleim, A.; Abdel-Rahman, E. M. & Heppler, G. R. (2011) A large-stroke electrostatic micro-actuator. *Journal of Micromechanics and Microengineering*, Vol. 21., No. 7., pp. 1-12.

Vagia, M.; Nikolakopoulos, G., & Tzes, A. (2008). Design of a robust PID-control switching scheme for an electrostatic micro-actuator. *Control Engineering Practice*. Vol. 16., No. 11., pp. 1321-1328.

Vagia, M. & Tzes, A. (2010a). LMI-region Pole Placement Control Scheme for an Electrostatically Actuated micro Cantilever Beam. *the 18th Mediterranean Conference on Control and Automation (MED 10).*, Congress Palace, Marrakech, Morocco, pp. 231-236.

Vagia, M. & Tzes, A. (2010b). A Literature Review on Modeling and Control Design for Electrostatic Microactuators with Fringing and Squeezed Film Damping Effects. *Proceedings of American Control cofnerence 2010.*, Baltimore, Maryland, US, pp. 3390-3402.

Younis, M.; Abdel Rahman, E. M. & Nayfeh, A. H. (2003). A reduced order model for Electrically Actuated Microbeam-Based MEMS. *Journal of Microelectromechanical Systems.*, Vol. 12., No. 5., pp. 672-680.

PID Controller Design Approaches - Theory, Tuning and Application to Frontier Areas

Edited by Dr. Marialena Vagia

ISBN 978-953-51-0405-6
Hard cover, 286 pages
Publisher InTech
Published online 28, March, 2012
Published in print edition March, 2012

First placed on the market in 1939, the design of PID controllers remains a challenging area that requires new approaches to solving PID tuning problems while capturing the effects of noise and process variations. The augmented complexity of modern applications concerning areas like automotive applications, microsystems technology, pneumatic mechanisms, dc motors, industry processes, require controllers that incorporate into their design important characteristics of the systems. These characteristics include but are not limited to: model uncertainties, system's nonlinearities, time delays, disturbance rejection requirements and performance criteria. The scope of this book is to propose different PID controllers designs for numerous modern technology applications in order to cover the needs of an audience including researchers, scholars and professionals who are interested in advances in PID controllers and related topics.

InTech Europe
University Campus STeP Ri
Slavka Krautzeka 83/A
51000 Rijeka, Croatia
Phone: +385 (51) 770 447
Fax: +385 (51) 686 166
www.intechopen.com

InTech China
Unit 405, Office Block, Hotel Equatorial Shanghai
No.65, Yan An Road (West), Shanghai, 200040, China
中国上海市延安西路65号上海国际贵都大饭店办公楼405单元
Phone: +86-21-62489820
Fax: +86-21-62489821

IntechOpen